Journal of Ceramic Processing Research. Vol. 21, No. 5, pp. 565~570 (2020)
(Received 22 April 2020, Received in revised form 5 June 2020, Accepted 10 June 2020)
https://doi.org/10.36410/jcpr.2020.21.5.565

J O U R N A L O F
Ceramic Processing Research

Quadratic magnetoelectric effect of barium titanate-cobalt ferrite (0-3) ceramic composite

Morad Etier* and Hesham Almomani
Industrial Engineering Department, The Hashemite University, Zarqa 13133, Jordan

In this research, the quadratic magnetoelectric effect for different compositions of barium titanate cobalt ferrite ceramic composites has been reported. Structural analysis was firstly demonstrated using different techniques e.g. x-ray diffraction and scanning electron microscopy, then both the first and the second order magnetoelectric effects were measured and analyzed. It was shown that the magnetic, ferroelectric and magnetoelectric properties of the ceramic composites depend mainly on the weight percentage of the constituents. Sample of 50% weight of barium titanate gave the highest longitudinal and traverse magnetostriction. The maximum induced magnetization as a function of electric field was observed for the sample contains 50% weight of barium titanate with a second order magnetoelectric coupling coefficient value $\gamma_{333} = 20 \times 10^{-18}$ *s/V*. This value is considered to be the first estimated quadratic magnetoelectric effect value for a composite material.

Keywords: Mutliferroics, Quadratic magnetoelectric effect, (0-3) Composite.

Introduction

Composites are interesting nowadays due to the new properties resulting from the combination of two materials, i.e combination of ferroelectric with ferromagnetic material to produce magnetoelectrics (MEs). These materials can be polarized by magnetic field and magnetized by electric effect which correspond to the direct and the converse magnetoelectric effect, respectively. Sensors, MERAMs, transformers, energy harvesters and electric field tunable devices are the main possible applications for the ME materials [1-5]. In single phase magnetoelectric materials, the low values of the ME effect restrict their technological applications. On the other hand, composites that combine piezomagnetism and piezoelectricity still an adequate option for optimizing the effect, because of the variety of synthesizing methods, structures and properties. This may inspire researchers for finding the optimum conditions in order to gain better results. In theory, the direct and the converse magnetoelectric effect are obtained from the derivative of the free energy (F) of a system with respect to both electric and magnetic fields as follows [6]:

$$P_i = -(\delta F/\delta E) = \alpha_{ij}H_j + (\beta_{ijk}/2)H_jH_k + \ldots$$

(Direct ME effect) (1)

$$\mu_o\mu_i = -(\delta F/\delta H) = \alpha_{ji}E_j + (\gamma_{ijk}/2)E_jE_k + \ldots$$

(Converse ME effect) (2)

*Corresponding author:
Tel : +962 (5) 3903333-5013
Fax: +962 (5) 3826613
E-mail: morad.etier@hu.edu.jo

where P, M are the electric polarization and the magnetization, respectively. H and E are the magnetic and the electric fields, respectively, and μ_o is the magnetic constant. The first order magnetoelectric effects (α_{ij} or α_{ji} [unit s/m]) are the induced magnetization by electric field $M(E)$, or the induced polarization by magnetic field $P(H)$, respectively. In case of the second order magnetoelectric effect (β_{ijk} [unit s/A] and γ_{ijk} [unit s/V]) are the change of dielectric permittivity with respect to magnetic field $\varepsilon(H)$ or the variation of permeability by electric field $\mu(E)$ [7]. Using equations (1) and (2), the second order ME effect γ_{ijk} is proportional to the square of the applied electric field $\gamma = (2\mu_o\Delta M)/(\Delta E)^2$ while β_{ijk} is proportional to the square of the applied magnetic field $\beta = (\Delta p)/(\Delta H)^2$. Utilizing these equations, the first one γ is more clear in the converse ME effect, because it depends on the applied electric field, while the second one β appears in the direct ME measurement because it depends on the applied magnetic field. Both the first and the second order magnetoelectric effect can be detected experimentally in the same material. Previously, it was reported that the second order ME effect for single phase materials was experimentally measured for lithium ferrite ($LiFe_5O_8$) and Yttrium Iron Garnet YIG ($Y_3Fe_5O_{12}$) in the low-temperature interval 4-100K [8-10]. In composites, the magnetoelectric effect depends on the linear piezoelectric effect of the first constituent which is usually ferroelectric, and also on the nonlinear magnetostrictive effect of the second one which is ferromagnetic. For that reason, one should expect linear and nonlinear magnetoelectric effect obtained from the combination of ferromagnetic/ferroelectric

magnetoelectric composites. Most of the magnetoelectric studies for composites with piezomagnetic-piezoelectric phases are carried out for the linear effect where the ac electric field or voltage is measured as a function of ac magnetic field. Different connectivies of magnetoelectrics have been synthesized and analyzed including the (0-3), (1-3) and (2-2) structures [11-13]. These structures included, sintered ceramic samples, epitaxial thick and thin films, pillars and others. The interaction between the piezoelectrics and the piezomagnetics in such structures is crucial factor to produce the magnetoelectric effect. Among these structures, the (0-3) connectivity still a good option in order to give isolated magnetic grains distributed inside a ferroelectric matrix. This can provide more interaction areas between the phases, excellent poling and accomplished strain mediated transfer capabilities. However, different approaches were empolyed to synthesize (0-3) composites including sol-gel and sintering technique, pulsed laser deposition and epoxy bonding of layers. In literature, several materials were selected to synthesize magnetoelectric composites, for examples, PZT/NFO epitaxial heterostructure [14],

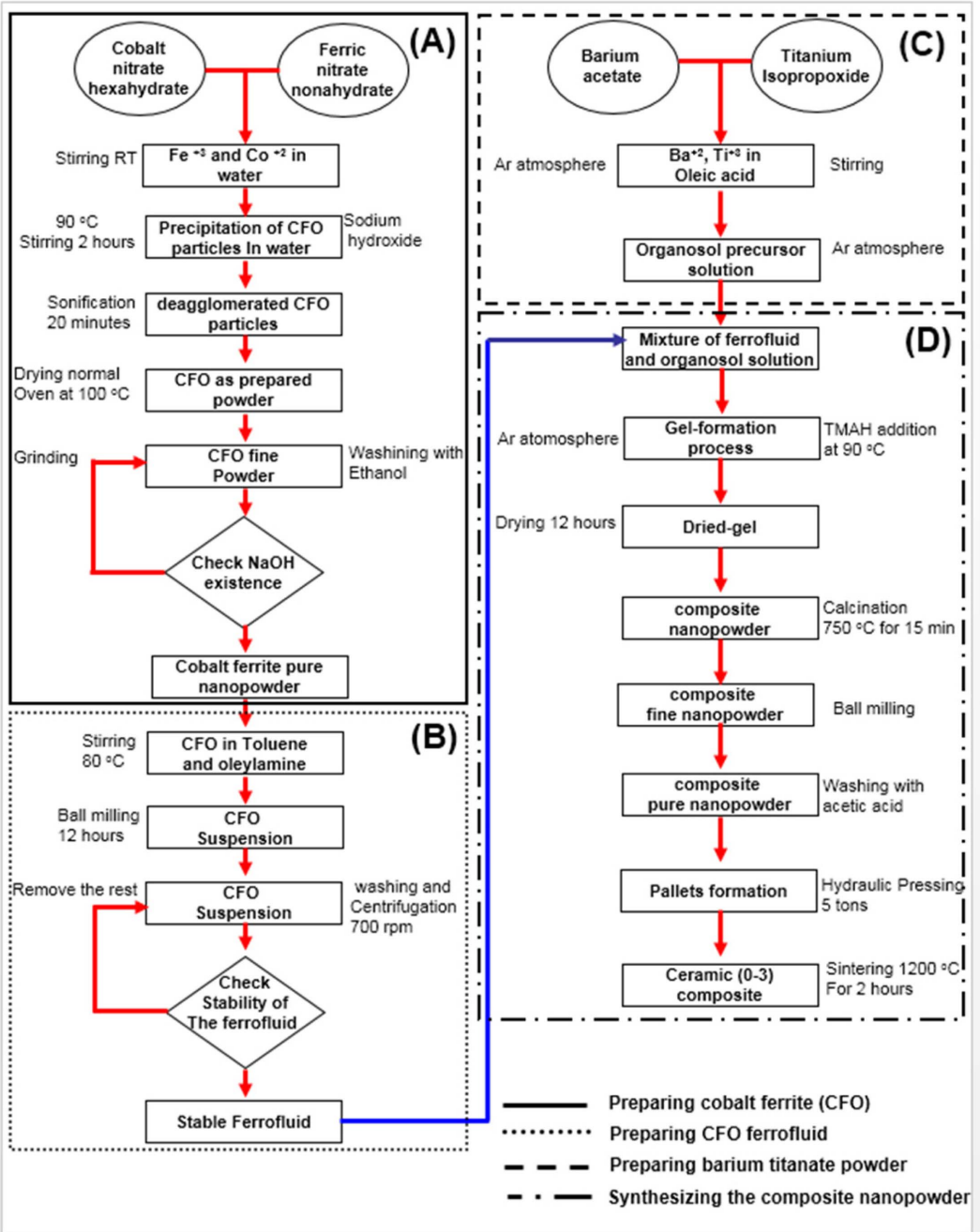

Fig. 1. Detailed experimental procedures for producing xBTO-(1-x)CFO composites showing sequence (A) synthesizing method of cobalt iron oxide nanoparticles by co-precipitation method, sequence (B) preparation of CFO ferrifluid, sequence (C) preparation of barium titanate nano powder and sequence (D) formation of composite nanopowder and until sintering to reach the (0-3) ceramic.

CFO/BTO core shell structure [15], PMN-PT/Terfenol-D plate [16], PZT-NFO-PZT thin films [17] and many others. Barium titanate (BTO) and cobalt ferrite (CFO) have excellent piezoelectric and piezomagnetic properties for the application of electric and magnetic sensors, respectively. For composites, the nonlinear magnetoelectic effect was reported as a voltage coefficient quadratic effect β_{ijk} which appeared in the direct magnetoelectric effect for different materials [18-20]. To our knowledge the second order ME effect in composites (γ_{ijk}) is not reported for such systems nor for other composites. In this article and for the first time, the values of the second order of the ME effect γ_{ijk} for different composition of xBTO-(1-x)CFO system were measured and reported. The values of the second order magnetoelectric effect are detected for such systems based on the converse magnetolectric effect experiment setup.

Materials and Methods

The detailed procedure for synthesizing the composites are shown in Fig. 1. The co-precipitation method was used to synthesize cobalt iron oxide nanoparticles using the same molar ratio of $Fe(NO_3)_3 \cdot H_2O$ and $Co(NO_3)_2 \cdot 6H_2O$ in water. The precipitation of cobalt ferrite particles was started after the addition of sodium hydroxide at 90 °C. The detailed sequence is shown in flowchart (A) in Fig. 1. Several times of ethanol washing can remove the rest of sodium hydroxide which may remain in the solution. The powder was sonificated for 20 min to reduce the particles' agglomeration then dried at 100 °C for 2 h. Inside an argon atmosphere, barium titanate precursor solution was prepared using barium acetate $Ba(C_2H_3O_2)_2$ and titanium isopropoxide $TiC_{12}H_{28}O_4$ in oleic acid (flowchart C in Fig. 1). An organosol precursor was formed where ions of titanium and barium are dissolved in oleic acid under magnetic stirring. Flowchart (B) in Fig. 1 shows the procedure for preparing cobalt ferrite stable ferrofluid, where the cobalt ferrite nanopowder synthesized in flowchart A was added into a solution of olyamine and toluene at 80 °C under magnetic stirring. Then, the solution was introduced to the ball milling machine for 12 h in order to deagglomerate the particles and reduce the particle size. After several times of centrifugation and washing, well suspended particles of cobalt ferrite particle in liquid were obtained. After that, adequate amount of this ferrofluid contains 40 nm of cobalt ferrite nanoparticles was prepared and added to barium titanate precursor solution obtained in flowchart C. The amount of cobalt in the ferrofluid was measured in order to give different weight percentage of the final powder comparing to the barium titanate amount. The stable ferrofluid and the barium titanate organ sol precursor were mixed together and an amount of Tetramethylammoniumhydroxide (TMAH) was added at 90 °C in order to promote the gelation process. The two phase precursor was well mixed using ball milling for 12 h and then calcined at 750 °C for 15 min (flowchart (D) in Fig. 1). To separate the particles and to prevent agglomeration, the powder was repeatedly milled using different sizes of ball milling then pressed using hydraulic press (2496 MPa) to form pallets. The samples were fired in normal oven at temperature 1,200 °C for 2 h. The pallets ceramic samples (5 mm in diameter and 0.5 mm thickness) were well polished in order to remove any undesirable layers. The structural analysis of the ceramic sample were investigated using x-ray diffraction (Siemens D-5000, BRUKER) with Cu-Kα radiation and λ = 1.54056 A°. Then the surface analysis and morphology were analyzed using scanning electron microscopy (SEM) (Quanta 400 FEG) with EDX capabilities. Magnetostriction of the samples were measured in both parallel and perpendicular directions using strain gauges connected onto the sample surfaces. After that two silver electrodes were painted onto the two faces forming a capacitor for magnetoelectric measurements. The electrically induced magnetic moments produced by variable electric field were measured by a modified SQUID susceptometer [21]. The measurements were carried out where the dc magnetic field and the ac electric field are perpendicular to the sample surface. The second order magnetoelectric effect values were extracted for all samples utilizing the quadratic equation fit for the induced magnetization versus ac electric field relations.

Results and Discussions

Room temperature x-ray diffraction patterns for different samples of xBTO-(1-x)CFO (x = 0.5, 0.6, 0.7, 0.8) are shown in Fig. 2. The patterns confirmed the existence of both barium titanate and cobalt ferrite phases. The peaks of the patterns coincide the peaks of both spinell cubic structure of ferromagnetic cobalt iron oxide with card ID (JCPDS 22-1086), and the

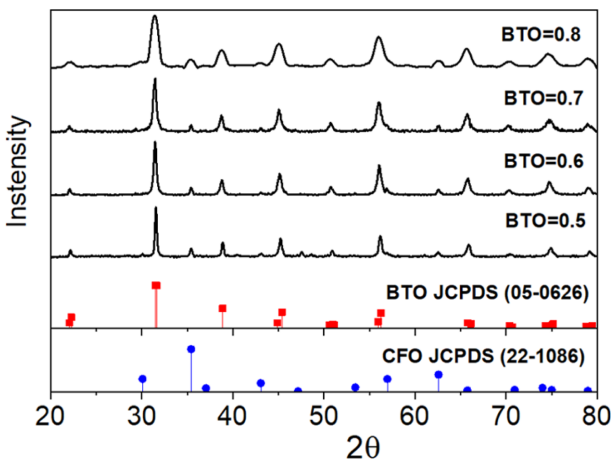

Fig. 2. X-ray diffraction patterns for different compositions of ceramic samples of barium titanate and cobalt ferrite composites.

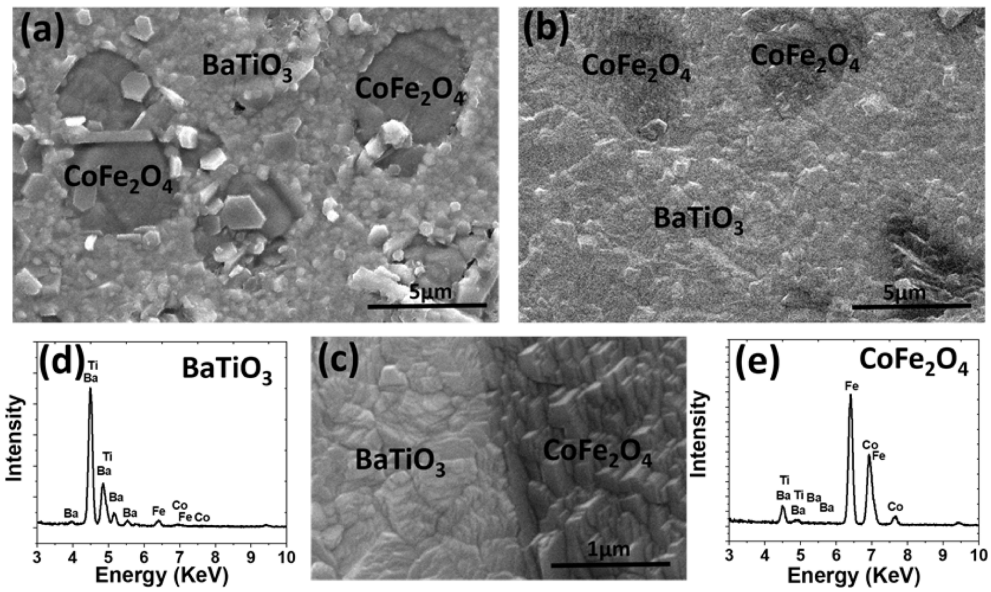

Fig. 3. Scanning electron micrographs for samples (a) x = 0.5 (b) x = 0.8 and (c) the interface between ferromagnetic and ferroelectric phases (d) energy dispersive spectroscopy for the barium titanate phase and (e) energy dispersive spectroscopy for cobalt ferrite phase.

tetragonal peroskite structure of ferroelectric barium titanate with card ID (JCPDS-0626) without any other interference phases. This is an indication of two distinct phases with no new other phases that may generate after high temperature sintering. Fig. 3 shows the surface morphology for the synthesized samples using the scanning electron microscopy. The separate distribution of the magnetic phases of cobalt ferrite (black regions) in barium titantate matrix (white regions) confirmed the (0-3) connectivity nature of the magnetoelectric ceramic samples (see Figs. 3(a) and 3(b)). The well-defined and strong interfaces between the constituents in composite magnetoelectric are prerequisites in order to enhance the magntoelectric effect [22]. Fig. 3(c) shows a magnification of the interface region between cobalt ferrite and barium titante. The two regions are well-connected without any cracks or porous areas. The elemental composition of the selected area was collected using energy dispersive spectroscopy. Pure elements of Ba, Ti, Co, Fe are detected in the regions (see Fig. 3(d) for barium titanate region and Fig. 3(e) for cobalt ferrite region).

The concept of magnetoelectric effect α_{ij} is based on the product properties obtained by a combination of two phases such as magnetostrictive and piezoelectric phases as shown in the following equation:

$$\alpha_{ij}=\frac{\mu_o dH_i}{dE_j}=\frac{\mu_o dH_i}{d\sigma_{mn}}\cdot\frac{d\sigma_{mn}}{d\varepsilon_{kl}}\cdot\frac{d\varepsilon_{kl}}{dE_j}=q_{imn}\cdot C_{mnkl}\cdot d_{jkl} \qquad (3)$$

where σ_{mn} and ε_{kl} are the stress and the strain tensors, respectively, d_{jkl}, C_{mnkl} and q_{imn} are the piezoelectric coefficient, stiffness and piezomagnetic coefficient tensors, respectively. Fig. 4(a) shows the magneto-striction plots measured parallel to applied external magnetic field. It is clear that the magnetostriction increased by increasing the content of the magnetic phase in the samples. Maximum value of strain was recorded for the sample of pure cobalt ferrite with values about -110 ppm. On the other hand, the maximum value of magnetostriction of composites was measured for the sample containing 50 percentage of barium titatate with value about -40 ppm, these values are comparable with values reported by Hrib et al. [23]. The low value of magnetostriction of composite comparing to pure cobalt ferrite may be attributed to the compression of barium titanate grains on the cobalt ferrite ones which may reduce the overall magnetos-triction. Fig. 4(b) shows the magnetostriction of the samples measured perpendicular to the external applied magnetic field. Lower values of magnetostriciton were measured with maxiumum value for pure cobalt ferrite (≈25 ppm). The lower values of magnetostriction obtained when the magnetic field perpendicular to the applied magnetic field are attributed to the magnetocrystalline anisotropy of cobalt ferrite [24].

Previously, the converse linear magnetoelctric effect α_{ji} values for different compositions were measured and reported [25]. An example of the electrically induced magnetization of the composite xBTO-(1-x)CFO when x = 0.7 in the electric field range (0-350 kV/m) is shown in Fig. 5. The relation between the induced magnetization and the electric field is linear where $\mu_o\mu_i = \alpha_{ji}E_j$. The linearity of the magnetoelectric effect was approved by different researchers and for different materials [26-28]. In order to investigate the degree of linearity of the ME effect, the curve was fitted using linear regression equation as shown in Fig. 5(a) and

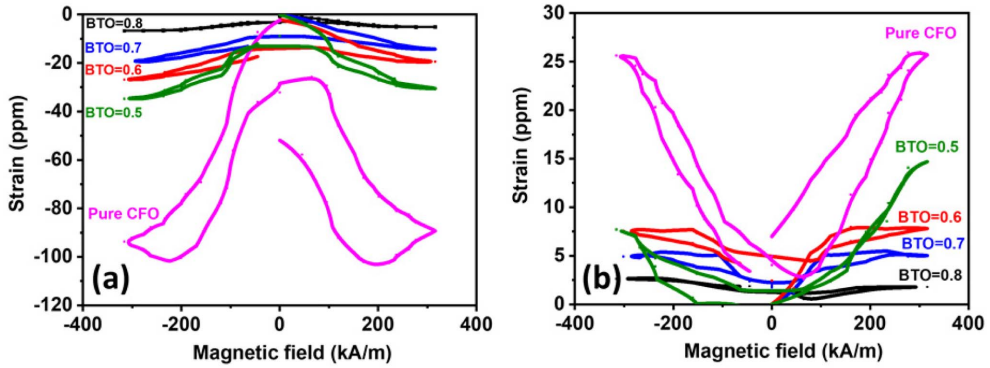

Fig. 4. Magnetostriction of barium titanate/cobalt ferrite composites (a) measured along the direction of the external applied magnetic field (b) measured perpendicular to the external applied magnetic field.

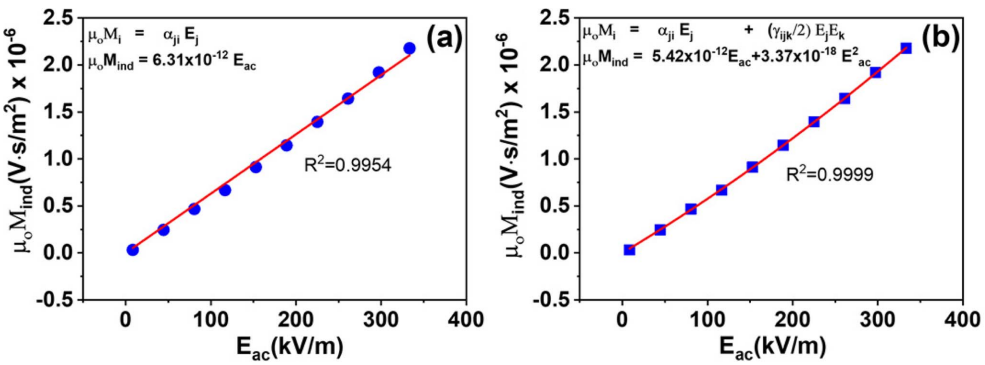

Fig. 5. Room temperature induced magnetic moments as a function of applied electric field, for composition x = 0.7 showing (a) linear equation fit (b) quadratic equation fit (f = 3 Hz, Hdc = 1500 Oe).

quadratic equation (Fig. 5(b)). It was shown that the quadratic equation fitted the curve perfectly with R-square value 0.9999 which is an indication of the appearance of the second order ME effect (γ_{ijk}). For the second order magnetoelectric effect γ_{ijk}, it is known that this effect depends mainly on the square of the electric field as indicated in Eq. (2) (see Fig. 5(b)).

For more explanation, the electric field was applied to the sample perpendicular to the sample surface so that the converse magnetoelectric effect - as shown in equation number (2)- can be calculated considering the applied electric field vector E_3=(0,0,E_3), so:

$$\mu_o M_3 = \alpha_{13}E_1 + \alpha_{23}E_2 + \alpha_{33}E_3 + (\gamma_{311}E_1^2 + \gamma_{312}E_1E_2 + \gamma_{313}E_1E_3 + \gamma_{321}E_2E_1 + \gamma_{322}E_2^2 + \gamma_{323}E_2E_3 + \gamma_{332}E_3E_2 + \gamma_{333}E_3^2) / 2$$

So that the applied equation for both first and second order magnetoeelctric effect is:

$$\mu_o M_3 = \alpha_{33}E_3 + (\gamma_{333}E_3^2) / 2 \quad (4)$$

Then, the values of first order ME effect α_{33} can be calculated by dividing the induced magnetization on the electric field and the unit will in s/m, and the value of γ_{333} can be calculated by dividing the induced magnetization by the square of electric field, so that the unit of the second order magnetoelectric effect γ will in s/V. To our knowledge, this unit of quadratic magnetoelectric effect has not been measured for any composite magnetoelectric material, while it has rarely been reported but for single phase materials only. The sample procedures for fitting curves were followed for the set of different compositions of xBTO-(1-x)CFO where (x = 0.5, 0.6, 0.7 and 0.8). Then, the quadratic magnetoelectric effect for different compositions was extracted and shown in Fig. 6. The same as the first order magnetoelectric effect, it is clear that the effect depends on the composition between the ferroelectric and ferromagnetic phases, where the greatest value was recorded for the composition when x = 0.5. This can be explained by larger interfaces between the two phases can be obtained when the fifty percent of the composite are ferromagnetics distributed in ferroelectric matrix, and hence, more strain generated by electrostriction and transferred to piezomagnetic phase [29]. The maximum room temperature value of the quadratic magnetoelectric effect γ at x = 0.5 reached to about 20×10^{-18} s/V whereas the value of 6.46 ps/MV was measured for $Co_4Nb_2O_9$ single crystal and at 10K [30]. The quadratic magnetoelectric effect of the barium titanate cobalt ferrite composite is three times larger than the single phase values and even at room temperature. We believe that having (0-3) composites, the

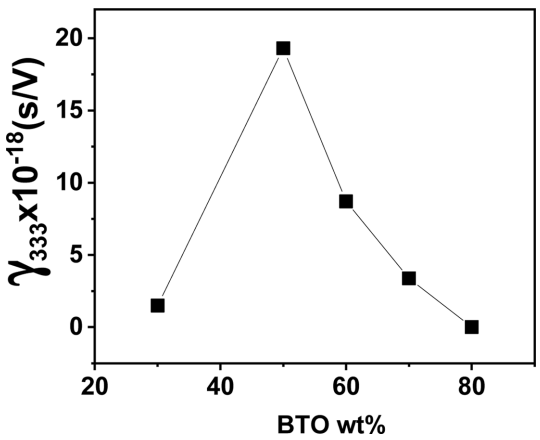

Fig. 6. Room temperature second order (γ) magnetoelectric effect for different composition of xBTO-(1-x)CFO composites measured at H_{dc} = 1500 Oe, f = 3 hz.

interface between the two phases with 50% weight percent will be higher and consequently give higher linear and quadratic ME effect as indicated in Fig. 6. The results obtained from this paper may be utilized by other researchers in order to measure linear and quadratic magnetoelectric effect for other composites with other phase connectivity.

Conclusion

In summary, the quadratic magnetoelectric effect for different compositions of barium titante and cobalt ferrite ceramic composites has been successfully extracted by the employment of fitting quadratic equation of the first order one. The values of the quadratic magnetoelectric coupling coefficient (γ) in unit of S/V were reported for the first time for a composite material. The maximum value of the quadratic magnetoelectric coupling coefficient for such composite was recorded when the weight percentage of barium titanate is 50% of the total composite weight with a value of $\gamma_{333} = 20 \times 10^{-18}$ *s/V*. The same as the first order magnetoelectric effect, it was also shown that the quadratic magnetoelectric effect depends on the constituents amounts of the ferroelectric/ferrimagnetic phases too. The existence of both the first and the second order magnetoelectric effect is beneficial for future applications such as the nonlinear magnetoelectric devices. This study inspires other researchers to study the relationship between the first and the second order ME effect in composites rather than single phases magnetoelectrics.

References

1. Y.K. Fetisov, D.A. Burdin, D.V. Chashin, and N.A. Ekonomov, IEEE Sens. J. 14 (2014) 2252-2256.
2. M. Bibes and A. Barthelemy, Nat. Mater. 7 (2008) 425-426.
3. S. Dong, J.F. Li, and D. Viehland. Appl. Phys. Lett. 85 (2004) 3534.
4. T. Onuta, Y. Wang, C.J. Long, and I. Takeuchi, Appl. Phys. Lett. 99 (2011) 203506.
5. C. Pettiford, S. Dasgupta, J. Lou, S.D. Yoon, and N.X. Sun, IEEE T. Magn. 43 (2007) 3343-3345.
6. M. Fiebig, J. Phys. D: Appl. Phys. 38 (2005) R123.
7. L. Mitoseriu, J. Span. Cer. Glas. Soc. 44 (2005) 177-184.
8. M. Mercier, G. Velleaud, and J. Puvinel, Physica B+C. 86-88 (1977) 1089-1090.
9. J. Cardwell, Phys. Status Solidi B. 45 (1971) 597.
10. S. Takano, E. Kita, K. Siratori, K. Kohn, S. Kimura, and A. Tasaki, J. Phys. Soc. Jpn. 60 (1991) 288-293.
11. F.L. Zabotto, F.P. Milton, A.J. Gualdi, A.J.A. de Oliveira, J.A. Eiras, and D. Garcia, J. Alloy Compd. 829 (2020) 154517.
12. G. Jian, H. Shao, C. Yan, N. Zhao, B. Song, and C.P. Wong, J. Magn. Magn. Mater. 449 (2018) 263-270.
13. H. Song, M. Peddigari, A. Kumar, S. Lee, D. Kim, N. Park, J. Li, D. R. Patil, and J. Ryu, J. Alloy Compd. 834 (2020) 155124.
14. Z. Zheng, P. Zhou, Y. Liu, K. Liang, R.G. Tanguturi, H. Chen, G. Srinivasan, Y. Qi, and T. Zhang, J. Alloy Compd. 818 (2020) 152871.
15. P. Kaviraj, R. Pramanik, and A. Arockiarajan, J. Ceram. Int. 45 (2019) 12344-12352.
16. K.Y. Fang, L.H. Gong, W.Q. Jing, and F. Fang, Mater. Today Commun. 21 (2019) 100650.
17. L. Jian, A.S. Kumar, C.S. Chitra Lekha, S. Vivek, I. Salvado, A. L. Kholkin, and S.S. Nair, Nano Structures and Nano. Objects. 18 (2019) 100272.
18. D.A. Burdin, D.V. Chashin, N.A. Ekonomov, L.Y. Fetisov, Y.K. Fetisov, G. Sreenivasulu, and G. Srinivasan, J. Magn. and Magn. Mat. 358-359 (2014) 98-104.
19. J. Ma, Z. Li, Y. Lin, and C.W. Nan, Magn and Magn. Mater. 323 (2011) 101-103.
20. Y. Wang, Y. Shen, J. Gao, M. Li, J. Li, and D. Viehland, Appl. Phys. Lett. 102 (2013) 102905.
21. P. Borisov, A. Hochstrat, V.V. Shvartsman, and W. Kleeman, J. Rev. Sci. Instr. 78 (2007) 106105.
22. C.-W. Nan, M.I. Bichurin, S. Dong, D. Viehland, and G. Srinivasan, J. of appl. phys. 103 (2008) 031101.
23. L.M. Hrib and O.F. Caltun, J. Alloy. Compd. 509 (2011) 6644-6648.
24. R.M. Bozorth and J.G. Walker, Phys. Rev. 88 (1952) 1209.
25. M. Etier, V.V. Shvartsman, S. Salamon, Y. Gao, H. Wende, and D.C. Lupascu, J. Amer. Cer. Soc. 99 (2016) 1-9.
26. P. Yanda, N.V. Ter-Organessian, and A. Sundaresan, J. Phys. Rev. B. 100 (2019) 104417.
27. X. Shen, L. Zhou, Y. Chai, Y. Wu, Z. Liu, Y. Yin, H. Cao, C. Cruz, Y. Sun, C. Jin, A. Munoz, J. Alonso, and Y. Long, J. NPG Asia Mat. 11 (2019) 50.
28. D. Viehland, M. Wuttig, J. McCord, and E. Quandt, MRS Bull. 43 (2018) 834-840.
29. Y. Wang, J. Hu, Y. Lin, and C.-W. Nan, NPG Asia Mat. 2(2010) 61-68.
30. Y. Cao, G. Deng, P. Beran, V Feng, B. Kang, J. Zhang, N. Guiblin, B. Dkhil, W. Ren, and S. Cao, Sci. Rep. 7 (2017) 14079.